DEPARTMENT OF MECHANICAL ENGINEERING
COLLEGE OF ENGINEERING & TECHNOLOGY
OLD DOMINION UNIVERSITY
NORFOLK, VIRGINIA 23529

A QUIET TUNNEL INVESTIGATION OF HYPERSONIC BOUNDARY-LAYER STABILITY OVER A COOLED, FLARED CONE

Principal Investigator: Gregory V. Selby

Final Report
For the period ended February 15, 1996

Prepared for
National Aeronautics and Space Administration
Langley Research Center
Hampton, VA 23681-0001

Under
Research Grant NCC1-180
Stephen P. Wilkinson, Technical Monitor
FLDMAD-Flow Modeling and Contracts Branch

Submitted by the
Old Dominion University Research Foundation
P.O. Box 6369
Norfolk, VA 23508-0369

September 1996

ACKNOWLEDGMENTS

The attached paper entitled, "A Quiet Tunnel Investigation of Hypersonic Boundary-Layer Stability Over a Cooled, Flared Cone" is being submitted in lieu of a final report for the research project entitled, "Computational and Experimental Parametric Study of Transition at High Mach Numbers," supported by the National Aeronautics and Space Administration, research grant NCC1-180, Stephen P. Wilkinson, of FLDMAD-Flow Modeling and Contracts Branch was technical monitor.

A QUIET TUNNEL INVESTIGATION OF HYPERSONIC BOUNDARY-LAYER STABILITY OVER A COOLED, FLARED CONE

Alan E. Blanchard* and Gregory V. Selby†,
Old Dominion University, Norfolk VA

and Stephen P. Wilkinson‡
NASA Langley Research Center, Hampton VA

Abstract

A flared-cone model under adiabatic- and cooled-wall conditions was placed in a calibrated, low-disturbance Mach 6 flow and the stability of the boundary layer was investigated using a prototype constant-voltage anemometer. The results were compared with linear-stability theory predictions and good agreement was found in the prediction of second-mode frequencies and growth. In addition, the same 'N=10' criterion used to predict boundary-layer transition in subsonic, transonic, and supersonic flows under low freestream noise conditions was found to be applicable for the hypersonic flow regime as well. Under cooled-wall conditions, a unique set of spectral data was acquired that documents the linear, nonlinear, and breakdown regions associated with the transition of hypersonic flow under low-noise conditions.

Nomenclature

A = disturbance amplitude
A_0 = initial amplitude or amplitude at most upstream location
A-O-A = angle-of-attack
f = frequency, Hz
M = Mach number
N = integrated growth rate
P_0 = stagnation pressure, psia
Re_T = Transition Reynolds number
Re_∞ = unit Reynolds number, per foot
R_w = resistance of the hot-wire sensing element
$R_{w,adiabatic}$ = resistance of the hot-wire sensing element without heating
T_0 = stagnation temperature, °R
$V_{s,mean}$ = mean voltage of CVA output
$V_{s,RMS}$ = RMS voltage of CVA
x = distance along the axis on the cone, in.
y = distance normal to the x-axis, in.
δ = boundary layer thickness, in.
δ_T = thermal boundary layer thickness, in.

Introduction

The design of high-speed aircraft requires a knowledge of high-speed boundary-layer stability. To withstand the aerodynamic heating loads of hypersonic flight, an aircraft can incorporate cooling systems and/or advanced composite material construction. Designers must confidently estimate heating loads to select an appropriate, cost-effective solution to the aerodynamic heating problem. However, these heating loads as well as the aerodynamic performance of the aircraft depend on the laminar or turbulent state of the boundary layers. Consequently, an understanding and accurate modeling of turbulent flow evolution from the laminar state is a crucial factor in the design of high-speed aircraft.

Experimental high-speed flows are often contaminated by freestream disturbances.[1-4] Disturbance fields interact with boundary layers and produce conflicting results for similar models in different wind tunnels. For example, unexpected variations in Re_T were found for cone and flat plate models in different high-speed wind tunnels ($3<M<8$).[5,6] This result confirmed the undesirable effect of acoustic freestream disturbances and underscored the need for low-disturbance, high-speed tunnels also referred to as quiet tunnels.

Quiet-tunnel technology, developed and implemented at the NASA-Langley Research Center, maximizes the laminar flow region over the nozzle wall, thereby delaying the onset of

*Graduate Research Assistant, Department of Mechanical Engineering.

†Associate Professor and Chair, Department of Mechanical Engineering, Member AIAA.

‡Group Leader, Quiet Tunnel & Transition Group, Flow Modeling and Control Branch, Fluid Mechanics and Acoustics Division, Senior Member AIAA.

turbulence and the attendant radiated sound.[7-9] Part of the NASA-Langley program for hypersonic stability and transition research required the development of a quiet Mach 6 facility. This involved retrofitting a new quiet nozzle to the Nozzle Test Chamber facility and modifying the settling chamber. The modified facility is known as the Mach 6 Nozzle Test Chamber Facility (M6NTC). The nozzle was calibrated[10] and deemed suitable for the present boundary-layer stability investigation. Prior to the present research involving cooling effects and the preceding research of Lachowicz[11] for the adiabatic case, the Langley quiet tunnels were used primarily for transition studies.[12]

Despite their sparsity in the literature, significant high-speed stability experiments have been documented. Foremost is the recent serial work of Stetson, et al.,[13-23] which elucidated parametric effects, such as wall cooling, angle-of-attack, and nose bluntness, on the stability of high-speed flow. In terms of overall trends, these results agreed with linear-stability theory predictions; however, the tests were conducted in a conventional high-speed tunnel with typical freestream noise and transition was detected at a relatively low N~4 value.[24] In the progression of high-speed stability experimentation, the present research represents the next logical and anticipated advancement -- stability experiments in a quiet-flow environment.

The purpose of the present research was to conduct a parametric investigation of the stability of a flared cone boundary layer, with variable wall temperature, in a calibrated Mach 6 quiet flow and compare the results with theoretical predictions.[25] This comparison can reveal the extent of linear-stability theory (LST) as a valid predictor of instability phenomena in hypersonic flows. Moreover, as the boundary layer becomes turbulent, new information related to nonlinear instability can be obtained.

Experimental Apparatus

As shown in Fig. 1, the 91-6 Cone had a straight 5° angle for 6" which tangentially merged into a flared region of radius 91.443" for the remaining 12" of its length. The cone had a wall thickness of 0.080" and was instrumented with a ray of 51 T-type thermocouples diametric to a ray of 30 static pressure ports. All flow data were acquired above the thermocouple ray to facilitate direct comparison with wall temperature. The cone tip was 1.5" long (tip-radius ~0.0025") and the tip-frustum interface produced a 0.0005" rearward-facing step. The cone had a finish of 4-8 μin. RMS; however, sealant leakage from the tip-frustum interface produced ~10 randomly spaced roughness sites for 1.5">x>3" of height ~0.001".

The cone was equipped with internal passages for surface cooling with the frustum acting as a parallel-flow heat exchanger. The cone-tip was uncooled. A closed-loop temperature-controlled refrigerant system pumped low temperature coolant through insulated stainless steel tubing to the cone and back to the cooler for heat removal. During testing, the cooler set point was -15±1°C (465°R).

The operating parameters of the M6NTC were selected to match those of the numerical investigation at the highest practical Re_∞. For all tests, the tunnel operating parameters were T_0=810±3°R, P_0=130±2 psia, and M=5.91 (Re_∞=2.85x10^6/ft.). The quiet core length was 25.3" at this Re_∞ and began 20.76" downstream of the nozzle throat (throat-to-exit length=39.76").[10]

For the model placement shown in Fig. 1, a significant portion of the cone was in the 'quiet test core' of the nozzle with 3" of the cone extending beyond the nozzle exit. The tunnel could run indefinitely with the cone in this position. A mechanical approach was used to set the orientation of the cone to 0.0±0.1° angle-of-attack and yaw.

In order to acquire boundary-layer data, the first author designed and built unique hot-wire probes incorporating a contact sensor as shown in Fig. 2. The contact sensor on each probe was positioned ~0.035" downstream of the hot wire to minimize flow interference. After the contact sensor touched the cone surface, an automated traversing routine moved the wire to predetermined locations in the boundary layer where measurements were made. The hot-wire sensor was 0.0001" dia. platinum-rhodium (10%) wire with a length-to-diameter ratio of 150. To obtain the necessary curvature required to minimize unsteady strain gaging, the wire support tips were angled and

the wire was soldered, using high-temperature solder, to the center of the support tips.

The constant-voltage anemometer (CVA) used in the present research is a recent invention.[26-28] To reduce sensitivity variations due to overheat drift, the wire voltage was adjusted to maintain a mean resistance ratio ($R_w/R_{w,adiabatic}$) of 1.5 when acquiring data for spectral analysis. In Fig. 3, a typical no-flow noise spectra of the CVA is compared to a typical hot-wire spectra with the wire located in a low-disturbance region of the adiabatic-cone boundary layer. This figure illustrates: 1) the low noise level while operating in the M6NTC environment, and 2) the lack of unsteady strain gaging. Unsteady strain gaging would be seen as large amplitude spikes, often above 500 kHz. The roll-off of the no-flow noise output near 400 kHz defines the bandwidth of the CVA. Since CVA hot-wire calibration in compressible flows has not yet been rigorously studied and uncalibrated data were sufficient to determine the growth of the dominant frequencies, no attempt was made to calibrate the hot wires.

Standard measuring equipment was used to acquire the data. The time-trace data were acquired using a 12-bit digital oscilloscope with a sampling rate of 2 million points per second and record length of 2^{17} points. The CVA time-trace data were AC-coupled and filtered using a low-noise preamplifier with a low-pass filter setting of 1 MHz, a high-pass filter setting of 100 Hz, and a gain of 1. For each spectrum, the 2^{17} data points were divided into 2^8 records and averaged using an FFT length of 2^{10}. Due to the window length in the power spectral density (PSD) routine, the frequency amplitudes below 10kHz were suspect and are not presented. The units of the amplitudes of the PSD curves are $(volts)^2/Hz$ and all amplitudes presented are the square root of this parameter. A digital multi-meter/Scanner was used to measure mean and RMS voltage from the CVA and to measure hot-wire resistance. A data acquisition and control unit was used to acquire the voltages from the thermocouples and the resistance temperature devices.

Freestream Disturbances

To investigate the freestream flowfield outside of the boundary layers, the flow 0.24" above the model was surveyed (9"<x<16"). With a maximum δ of 0.055", the survey was at least 4 δ from the wall. Inviscid theory[29] predicts a shock 0.64" above the cone at x=6". Since the cone shock will move no closer to the cone surface as x increases, it is clear that the survey at y=0.24" was between the cone shock and the cone boundary layer.

In Fig. 4, the development of 'noisy' flow in the quiet tunnel is presented as a series of spectral plots for the x-locations investigated. There are no measurable disturbances in the flow until x=12.5", and this freestream noise contains only low frequency spectral components (in comparison to the higher second-mode frequencies). There are two generic features of the freestream noise field[18] illustrated by the 'noisy' flow curve at x=16.5": 1) the lowest frequencies have the highest amplitude, and 2) amplitudes rapidly diminish with increasing frequency. The spectral content of the 'noisy' flow at x=16.5" is typical of conventional tunnels. For the present research, the most important low-frequency disturbances were ~70 kHz, the first-mode frequency band.[25] There was a measurable 70 kHz disturbance in the freestream for x>14" that could trigger the growth of first-mode instabilities in the boundary layer. No second-mode frequencies were detectable in the freestream within the signal-to-noise ratio of the CVA. Hence, the M6NTC produced a substantial region of high-quality 'quiet' flow over the cone model absent the measurable freestream disturbances typical in a conventional tunnel.

Cone Wall Temperature

Temperature data derived from thermocouples mounted beneath the model surface provide a simple method of identifying the transition zones for hot-wire investigation. As a high-speed boundary layer undergoes transition, the heat transfer coefficient and hence the wall temperature increase.[30] Figure 5 presents wall temperature distributions, and the increase in temperature due to the presence of transitional flow is apparent.

The maximum wall-temperature peak in each case is an indicator of transition.[25] Under adiabatic-wall conditions, transition moved upstream from x=16" (B) in the quiet-flow case to x=11.5" (A) in the noisy-flow case. For 'noisy flow' generation, the M6NTC bleed slot suction valves were closed, creating turbulent flow over the nozzle walls which radiated acoustic disturbances into the freestream. The appreciable upstream movement of the transition point (a reduction in Re_T of one million) highlights the dependency of Re_T on freestream-noise levels and the value of quiet tunnels for transition and stability research.

For the cooled-wall case, large temperature gradients were present near the tip and base of the cone, but transition was discernible. Energy from the uncooled cone-tip conducted into the actively cooled region producing the negative temperature gradient for x<7". At x=7", the wall temperature attained the desired level of 470°R, roughly the set point of the cooler and lowest possible cone-wall temperature. The transition-related increase in wall temperature began at x=11" with transition identified at approximately x=15" (C). The 1" upstream movement of transition relative to the adiabatic-wall case (under quiet flow conditions) indicates the additional destabilizing effect of wall cooling over the pressure gradient effect. The cooled-wall temperature increased near the base of the cone (x>16") due to conduction effects from the relatively hot, uncooled sting mounting assembly.

Mean Flow

The first objective of the mean-flow investigation was to identify and compare δ with theoretical values. Since wire resistance increases approximately linearly with (total) temperature, the resistance of the unheated hot wire was recorded during traverses of the boundary layer. In Fig. 6, the resistance profile of the wire, normalized by the freestream value, is presented at x=9" for both the adiabatic- and cooled-wall cases. These R_w curves have the characteristic 'bulge' in T_0 near the boundary-layer edge (due to frictional heating[31]) typical of T_0 profiles in a compressible boundary layer. The location where R_w reaches the freestream value defines the experimental δ_T which is compared to the theoretical δ in Fig. 7. For x<15" in the adiabatic case and x<13" in the cooled-wall case, the δ_T trends compare well with δ for laminar boundary layers. The deviation of the δ_T trends from the laminar δ trends, evidenced by the increase in δ_T for x>15" in the adiabatic-wall case and x>13" in the cooled-wall case, reveals the growing, transitional nature of the boundary layers.

The second objective of the mean-flow investigation was to find evidence of mean-flow distortion. Since the resistance of a heated hot wire will respond to changes in mean mass flow and T_0, the mean CVA output voltage was recorded as the heated wire traversed the boundary layer. The CVA was operated at a constant wire voltage. In Fig. 8, the mean CVA output voltage, normalized by the y_{min} and y_{max} voltage values at each x location, is presented in contour plot form for both wall conditions. From Ref. 25, the laminar mean-flow quantities are known to change very slowly in the x-direction over the flared region of the cone; hence, nominally parallel contour lines would be expected in the laminar region. There are regions in both cases identified in Fig. 8 where parallel contours of mean CVA output exist, consistent with the expected laminar flow behavior. Downstream of the parallel contour regions, the contours appear to diverge at x=14" in the adiabatic-wall case and x=13" in the cooled-wall case, suggesting significant mean-flow distortion and fuller profiles at the transition locations (as defined in Fig. 5).

Fluctuating-Flow Overview

The fluctuating disturbances in the boundary layers were measured at the location of maximum disturbance energy. To determine the location of maximum disturbance energy, the heated hot wire at constant wire voltage traversed the boundary layers and the RMS voltage output of the CVA was recorded. In Fig. 9, the RMS data at x=9" is presented versus the y distance normalized by δ_T. The RMS maximum occurs near δ_T at $y/\delta_T \sim 0.9$ for both cases, which is typical of high-speed boundary layers.[23] The disturbance amplitude

rapidly diminishes to a constant noise value outside the boundary layer. Note the second maxima at $y/\delta \sim 0.55$. The spectral content of these peaks did not significantly differ from the dominant peaks and may result from an increasing hot-wire sensitivity combined with decreasing disturbance amplitude.

Spectral data were acquired at the locations of maximum RMS energy for both cases. In Figures 10 and 11, the spectral content of the unsteady data acquired under adiabatic-wall conditions are presented in oblique-view and front-view waterfall plots, respectively. Similar data is presented for the cooled-wall case in Figures 12 and 13. The A_o value used for normalizing each frequency was the value measured at x=9"--the most upstream location. As shown in the figures, there are three distinct spectral peaks common to both cases: 1) a peak at 0 kHz, 2) a peak coincident with the expected second-mode frequencies, and 3) a peak twice the second-mode frequency coincident with second-mode harmonics. Another noteworthy similarity of the data sets is the constancy of the second-mode frequency band as evidenced in Figures 11 and 13 (and consistent with theoretical predictions). In previous experimentation with a straight cone,[13] δ increased with x and hence the most unstable second-mode frequency shifted to lower frequencies via the well-known boundary-layer tuning effect of the second mode. As seen in Fig. 7, there is no significant change in δ over the region of interest, thereby ensuring that the most unstable second-mode disturbances are tuned to nominally constant frequencies.

Despite the similarities, there are significant differences in the data sets, the most obvious is the spectral filling between the peaks in the cooled-cone case at the end of the survey ($15" < x < 16.5"$). This spectral filling portends the inevitable evolution of an unremarkable turbulent flow spectrum without peaks.

Second-Mode Disturbances

Another significant difference in the two spectral data sets is the dominant second-mode frequencies and their growth. In Fig. 14, two spectra taken from the linear-growth region in each case are shown to facilitate identification of the dominant second-mode frequencies. The second-mode frequency band in the adiabatic-wall case appears to be composed of 275 and 291 kHz as the dominant frequencies with lesser contributions from 260 and 306 kHz. For the cooled-wall case, the second-mode frequency band is composed of a dominant 306 kHz frequency with lesser contributions from 291 and 320 kHz. Note especially that a pattern exists in the identified frequencies -- all may be considered harmonics of ~14.6 kHz. Changing the parameters of the PSD routine to refine the spectra only made the identifiable peaks more pronounced. This result differs from previous experimentation in which 'smooth' second-mode frequency bands were found without the remarkable peaks identified in the present data.

In Fig. 15, the growth of the dominant second-mode disturbances for both wall conditions (and for the 93-10 flared cone described in Ref. 11 under adiabatic wall conditions) is compared to the respective predicted growth of the dominant second-mode disturbances based on quasi-parallel LST.[25] The experimental data was shifted an arbitrary amount to match LST over its exponential growth region.

For the 91-6 cone data, there are two regions where the experimental amplitudes deviate from the predicted growth. At low amplitude (N=4.8 for the adiabatic wall and N=6.6 for the cooled wall), all potential second-mode disturbance amplitudes are lost in the instrumentation noise. The recorded amplitudes in this region are nominally constant and represent the 'no-flow' electronic noise level of the CVA. Once the amplitude of the disturbances rise above the noise level, the experimental growth matches well the predicted growth up to the saturation levels at N=9 at x=15" for the adiabatic-wall case and N=11 at x=13" for the cooled-wall case. Due to the limited extent of the survey for the adiabatic-wall 93-10 cone, the low-amplitude limit of the CVA was not reached, but saturation of the second-mode disturbance was evident at N=9 at x=18". Whereas LST assumes disturbances of negligibly small amplitude and hence infinite growth, physical reality dictates that the disturbances will grow to a finite amplitude preceding saturation and other 'nonlinear' phenomena[32] such as mean-flow distortion and harmonic generation. The main conclusion of

Fig. 15 is that there are significant 'linear' regions in the data presented where second-mode frequencies follow the predicted growth up to an N-factor of ~10.

Second-Mode Frequency Patterns

Although harmonic patterns of the most unstable second-mode frequencies were identified, the definitive source was not. This research was an uncontrolled natural stability experiment and it was assumed that unstable disturbances in the boundary layer originated in the freestream and entered the boundary layer via receptivity mechanisms.[33] From Fig. 4, there were no detectable freestream disturbances for f>130 kHz, yet a peculiar set of second-mode disturbances (f>260) were measured in the boundary layers under various wall conditions with an apparent harmonic relationship. The frequencies composing this set could be considered higher harmonics of a relatively low 14.6 kHz frequency which was a significant component of the freestream disturbance field. As shown in Fig. 16, perturbing the A-O-A modified the orientation of the cone boundary layer to the freestream-disturbance field, resulting in dominant frequencies of 299 and 311 kHz on the windward ray -- these may be considered harmonics of a 12 kHz fundamental. (Note that this frequency increase is an excellent example of the second-mode frequency tuning to the 7% reduction in δ found on the windward ray.) Though an undetected experimental error must be included as a probable explanation for the pattern of dominant second-mode frequencies in this unique stability experiment, the variation in frequency pattern with A-O-A suggests that the pattern may depend upon fluid dynamic parameters. Future hypersonic quiet-tunnel stability experiments will be able to determine whether the observed frequency patterns are unique to quiet tunnels or are a function of the experimental methodology.

Low-Frequency Disturbances

In most high-speed experiments conducted in conventional tunnels, the freestream noise field is nearly constant, which results in a saturated low-frequency band in the spectra.[13] However, in this quiet-tunnel experiment, the amplitude of the freestream noise increases with downstream distance (see Fig. 4). In Fig. 17, the growth of the lowest frequency investigated (15kHz) is presented in the cooled-wall and adiabatic-wall boundary layers and in the freestream. As shown, the amplitudes of the 15 kHz disturbances in the boundary layers are higher than those in the freestream for all x, suggesting that these disturbances are being internalized at a rate greater than the damping rate or that a receptivity mechanism is at play. However, the cooled-wall relative amplitudes are everywhere higher than the adiabatic-wall amplitudes suggesting that the thinner cooled-wall boundary layer with faster growing disturbances was more receptive to the freestream noise than was the adiabatic-wall boundary layer. Since the geometry of the cone model included a flare, there was the possibility that the growth of the lowest frequencies could be related to the growth of Görtler vortices. However, if this were the case, then the Görtler instabilities were growing near the rate of the second mode--an unlikely prospect. The developing noise field in the quiet tunnel has revealed that low-frequency disturbances grow faster in the cooled-wall case than in the adiabatic-wall case.

Hypersonic Transition

Prior to this experiment, few experimental data sets in the hypersonic flow regime documented the evolution of linear disturbances into nearly turbulent flow. Under cooled-wall conditions, a unique spectral data set was acquired that shows an electronic noise level (no detectable disturbances), linear growth of second-mode disturbances, saturation, and breakdown into a developing turbulent flow.

Referring to Fig. 18 (a contour plot of the data in Figures 12 and 13), the linear region of the transition zone in the hypersonic boundary layer can be readily identified. Up to x=13", the primary second-mode instabilities grow linearly; i.e., independently and at exponential rates. The lower frequencies, presumably related to the internalization of freestream disturbances, also 'grow' independently in the linear region and do not interfere with the expected development of the primary instabilities. Noted is a distinct 50 kHz disturbance in the cooled-wall case with growth consistent with a first-mode instability,

but this disturbance is inconsequential compared to the role of second-mode disturbances in the transition process. Based on LST predictions, the boundary layer is unstable to second-mode disturbances starting at x~4" and are detected for x>10"; hence, the origin of the linear region may be bracketed to 4"<x<10".

For x>13", four indicators of nonlinear evolution are noted in the data: 1) saturation of the primary instability waves in Fig. 15; 2) existence of second-mode harmonics in Fig. 12; 3) evidence of mean-flow distortion in Fig. 8; and 4) boundary-layer growth above the laminar level in Fig. 7. The coexistence of saturated fundamental waves and higher harmonics with a distorted and growing mean flow may be considered indicative of vortical motion in the boundary layer. This large-scale swirling within the boundary layer causes rapid heating of the cone surface, noted by the increase in wall temperature as seen in Fig. 5, up to a maximum temperature at x=15". Downstream of x=15", the large-scale vortices presumably 'breakdown' into smaller scales evidenced by the rapid spectral filling as seen in Fig. 12. The beginning of the breakdown region is defined in Fig. 18.

In the nonlinear region, between the easily identifiable linear and breakdown regions, secondary instabilities generally introduce three-dimensionality to the transition process; however, secondary instabilities and nonlinear breakdown are "completely open questions" in high-speed flows.[23] One recent theory,[34] suggests that a turbulent spectrum may be generated by the interaction of oblique, finite-amplitude subharmonic instabilities with second-mode instabilities. In the cooled-cone data, there are no detectable subharmonic disturbances in the nonlinear region, so this potential transition mechanism does not present a plausible explanation for the observed breakdown. A recent experiment[11] documents possible subharmonics in the transition zone of a hypersonic boundary layer, but the preponderance of quiet-tunnel stability data (2 data sets in the present experiment and 2 of 3 data sets presented in Ref. 11) suggests that second-mode subharmonics are atypical hypersonic transition phenomena. The only discernible growth in the nonlinear region of this experiment is a spectral broadening of the dominant frequency bands. Due to its orientation with respect to the axisymmetric flow, the hot-wire sensor can only detect streamwise flow disturbances and is incapable of resolving possible azimuthal modes. Hence, the peculiar absence of a distinct and growing frequency band in the nonlinear region suggests that secondary instabilities may not have significant streamwise components. Based on this assumption, it is speculated that the spectral broadening of the disturbance bands in the nonlinear region may be due to a growing azimuthal-mode secondary instability which distorts the developing vortices into a pattern analogous to the K-type breakdown of Λ-vortices in the flow over a flat plate.[35] This azimuthal vorticity pattern that may develop is shown in Fig. 18. The flow disturbances at the end of the nonlinear region are thought to be a series of large-scale, three-dimensional vortices susceptible to the destructive interaction of possible tertiary instabilities[36] leading to turbulent breakdown.

Conclusions

The stability of the hypersonic boundary layer over a flared cone under adiabatic- and cooled-wall conditions has been investigated with $Re_\infty = 2.85 \times 10^6$/ft. in a quiet flow. Following are the significant conclusions related to this experiment:

1) The freestream above the boundary layer was found to be 'quiet' up to x=12.5"
2) The development of the freestream noise field followed typical trends with the lowest frequencies having the highest amplitudes with no measurable disturbances above 130 kHz.
3) In the 'linear' regions, the experimental δ_T in both cases compared well with the mean-flow calculation of δ.
4) In the adiabatic- and cooled-wall cases, the second-mode disturbances were found to be discrete frequencies with a possible harmonic relationship. It was not determined whether this was the result of experimental error or a hypothesized 'harmonic receptivity' mechanism.
5) In the adiabatic-wall case, the dominant second-mode frequencies were 275 and 291 kHz and grew to N=9, following the LST trend for 270 kHz.

6) In the cooled-wall case, the dominant second-mode frequency was 306 kHz which grew to N=11, following the LST trend for 310 kHz.
7) The saturation location of the disturbances showed that the N=10 transition-prediction guideline applies to hypersonic flows under low freestream noise conditions.
8) In the nonlinear region, it was speculated that azimuthal secondary instabilities could be growing and distorting the developing vortices prior to breakdown.
9) In the cooled-wall case, a breakdown region was identified downstream of the nonlinear region.
10) The low frequencies associated with freestream noise grew more rapidly in the cooled-wall case than in the adiabatic-wall case with growth similar to the growth of the respective second modes.
11) A peak in cone wall temperature was seen to occur near the end of the nonlinear region where the large-scale vortices were expected to have achieved maximum development just prior to breakdown.
12) The boundary-layer flow was shown to be very sensitive to angle-of-attack perturbations with the second-mode frequencies tuning to the boundary-layer thickness.

Acknowledgments

This research was supported by NASA-LaRC under Cooperative Agreement NCC1-180. The authors would like to thank J.T. Lachowicz for data-acquisition software support and Tao Systems for the use of a prototype CVA.

References

[1]Morkovin, Mark V., "On Transition Experiments at Moderate Supersonic Speeds," *Journal of the Aeronautical Sciences*, Vol. 24, No. 7, July 1957, pp. 480-486.

[2]Morkovin, M.V., "On Supersonic Wind Tunnels with Low Free-Stream Disturbances," *Journal of Applied Mechanics*, September 1959, pp. 319-324.

[3]Laufer, John, "Aerodynamic Noise in Supersonic Wind Tunnels," *Journal of the Aeronautical Sciences*, Vol. 28, No. 9, September 1961, pp. 685-692.

[4]Laufer, John, "Some Statistical Properties of the Pressure Field Radiated by a Turbulent Boundary Layer," *The Physics of Fluids*, Vol. 7, No. 8, August 1964, pp. 1191-1197.

[5]Pate, S.R., and Schueler, C.J., "Radiated Aerodynamic Noise Effects on Boundary-Layer Transition in Supersonic and Hypersonic Wind Tunnels," *AIAA Journal*, Vol. 7, No. 3, March 1969, pp. 450-457.

[6]Pate, S.R., "Measurements and Correlations of Transition Reynolds Numbers on Sharp Slender Cones at High Speeds," *AIAA Journal*, Vol. 9, No. 6, June 1971, pp. 1082-1090.

[7]Beckwith, I.E., Chen, F.-J., Wilkinson, S.P., Malik, M.R., and Tuttle, D., "Design and Operational Features of Low-Disturbance Wind Tunnels at NASA Langley for Mach Numbers from 3.5 to 18," AIAA Paper 90-1391.

[8]Wilkinson, S.P.; Anders, S.G.; Chen, F.-J. and Beckwith, I.E., "Supersonic and Hypersonic Quiet Tunnel Technology at NASA Langley," AIAA Paper 92-3908.

[9]Wilkinson, S.P., Anders, S.G., Chen, F.-J., and White, J.A., "Status of NASA Langley Quiet Flow Facility Developments," AIAA Paper 94-2498.

[10]Blanchard, A., Lachowicz, J., and Wilkinson, S., "Performance of the NASA-Langley Mach 6 Nozzle Test Chamber Facility," AIAA Paper 96-0441, Reno, Nevada, 1996.

[11]Lachowicz, J.T. and Chokani, N., "Hypersonic Boundary Layer Stability over a Flared Cone in a Quiet Tunnel," AIAA Paper 96-0782, Reno, Nevada, 1996.

[12]Chen, F. -J., Malik, M.R. and Beckwith, I.E., "Comparison of Boundary Layer Transition on a Cone and Flat Plate at Mach 3.5," AIAA Paper 88-0411, Reno, Nevada, 1988.

[13]Stetson, K., Thompson, E., Donaldson, J. and Siler, L., "Laminar Boundary Layer Stability Experiments on a Cone at Mach 8, Part 1: Sharp Cone," AIAA Paper 83-1761, Danvers, Massachusetts, 1983.

[14]Stetson, K.F., Thompson, E.R., Donaldson, J.C., and Siler, L.G., "Laminar Boundary Layer Stability Experiments on a Cone at Mach 8, Part 2: Blunt Cone," AIAA Paper 84-006, January 1984.

[15]Stetson, K.F., Thompson, E.R., Donaldson, J.C., and Siler, L.G., "Laminar

Boundary Layer Stability Experiments on a Cone at Mach 8, Part 3: Sharp Cone at Angle of Attack," AIAA Paper 85-0492, January 1985.

[16]Stetson, K.F., Thompson, E.R., Donaldson, J.C., and Siler, L.G., "Laminar Boundary Layer Stability Experiments on a Cone at Mach 8, Part 4: On Reynolds Number and Environmental Effects," AIAA Paper 86-1087, May 1986.

[17]Stetson, K., Thompson, E. and Donaldson, J., "Laminar Boundary Layer Stability Experiments On a Cone at Mach 8, Part 5: Tests with a Cooled Model," AIAA Paper 89-1895, Buffalo, New York, 1989.

[18]Stetson, K.F., Thompson, E.R., Donaldson, J.C. and Siler, L.G., "On Hypersonic Transition Testing and Prediction," AIAA Paper 88-2007.

[19]Stetson, Kenneth F. and Kimmel Roger L., "Example of Second-Mode Instability Dominance at a Mach Number of 5.2," AIAA Journal, Vol. 30, No. 12, December 1992, pp. 2974-2976.

[20]Stetson, K. and Kimmel, R., "Surface Temperature Effects on Boundary-Layer Transition," *AIAA Journal*, Vol. 30, No. 11, pp. 2782-2783.

[21]Stetson, K., "On Nonlinear Aspects of Hypersonic Boundary-Layer Stability," AIAA Journal, Vol. 26, No. 7, July 1988, pp. 883-885.

[22]Stetson, K.F., Thompson, E.R., Donaldson, J.C., and Siler, L.G., "A Comparison of Planar and Conical Boundary Layer Stability and Transition at a Mach Number of 8," AIAA Paper 91-1639, June 1991.

[23]Stetson, K. and Kimmel R., "On Hypersonic Boundary-Layer Stability," AIAA Paper 92-0737, Reno, Nevada, January 1992.

[24]Mack, L., "Stability of Axisymmetric Boundary Layers on Sharp Cones at Hypersonic Mach Numbers", AIAA Paper 87-1413, Honolulu, Hawaii, 1987.

[25]Balakumar, P. and Malik, M.R., "Effect of Adverse Pressure Gradient and Wall Cooling on Instability of Hypersonic Boundary Layers," High Technology Corporation, High Technology Report no. HTC-9404, March 1994.

[26]Sarma, Garimella, "Analysis of a Constant Voltage Anemometer Circuit," IEEE/IMTA Conference, Irvine CA, May 18-29, 1993.

[27]Mangalam, S.M., Sarma, G.R., Kuppa, S., and Kubendran, L.R., "A New Approach to High-Speed Flow Measurements Using Constant Voltage Anemometry," AIAA Paper 92-3957.

[28]Kuppa, S., Sarma, G.R. and Mangalam, S.M., "Effect of Thermal Inertia on the Frequency Response of Constant Voltage Hot Wire Anemometry and Its Compensation," FED-Vol. 161, *Fluid Measurement and Instrumentation*, ASME 1993, pp. 67-73.

[29]Ames Research Staff, "Equations, Tables, and Charts for Compressible Flow," NACA Report 1135, 1953.

[30]Scherrer, Richard, "Comparison of Theoretical and Experimental Heat-Transfer Characteristics of Bodies of Revolution at Supersonic Speeds," NACA Report 1055.

[31]Schlichting, H., *Boundary Layer Theory*, 7th ed., McGraw-Hill, New York, 1987.

[32]Reshotko, Eli, "Stability Theory as a Guide to the Evaluation of Transition Data," *AIAA Journal*, Vol. 7, No. 6, pp. 1086-1091.

[33]Arnal, D., "Boundary Layer Transition: Predictions Based on Linear Theory," AGARD-VKI Special Course on 'Progress in Transition Modeling', March-April 1993.

[34]Pruett, C.D. and Zang, T.A., "Direct Numerical Simulation of Laminar Breakdown in High-Speed, Axisymmetric Boundary Layers," AIAA Paper 92-0742, Reno, Nevada, 1992.

[35]White, F.M., *Viscous Fluid Flow*, McGraw-Hill, New York, 1991.

[36]Blanchard, Alan E. and Selby, Gregory V., "An Experimental Investigation of Hypersonic Boundary-Layer Stability in a Quiet Wind Tunnel," NASA Contractor Report 198287, February 1996.

List Of Figures

Figure #

Alan E. Blanchard, Figure 1

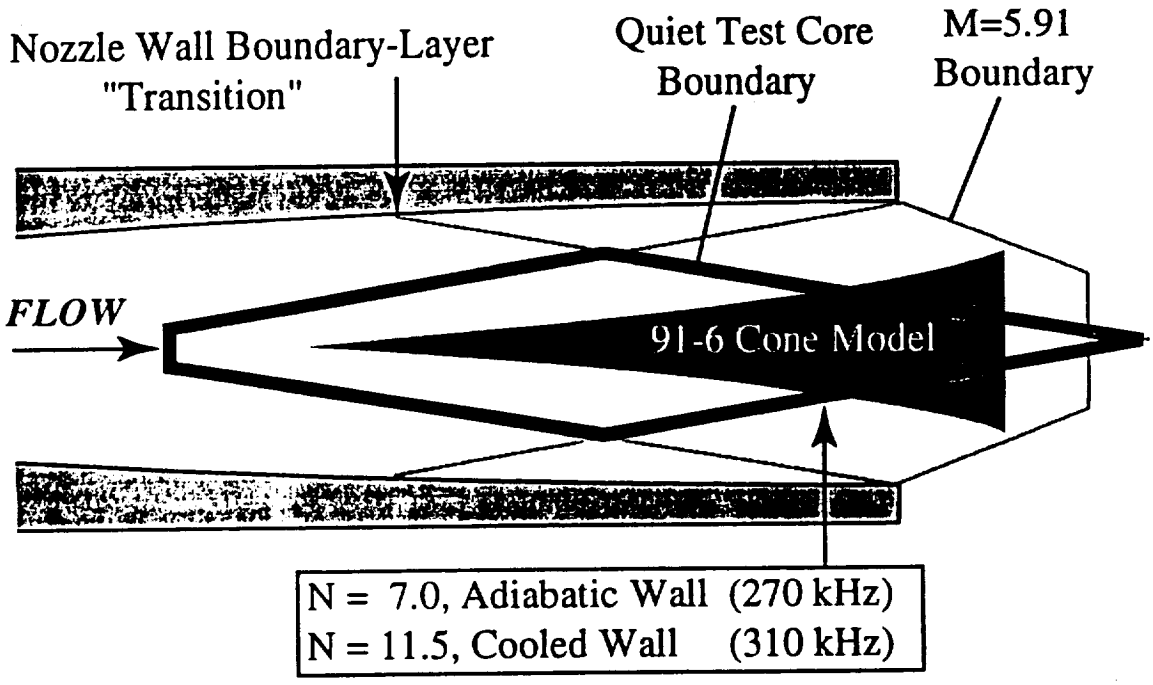

Alan E. Blanchard, Figure 2

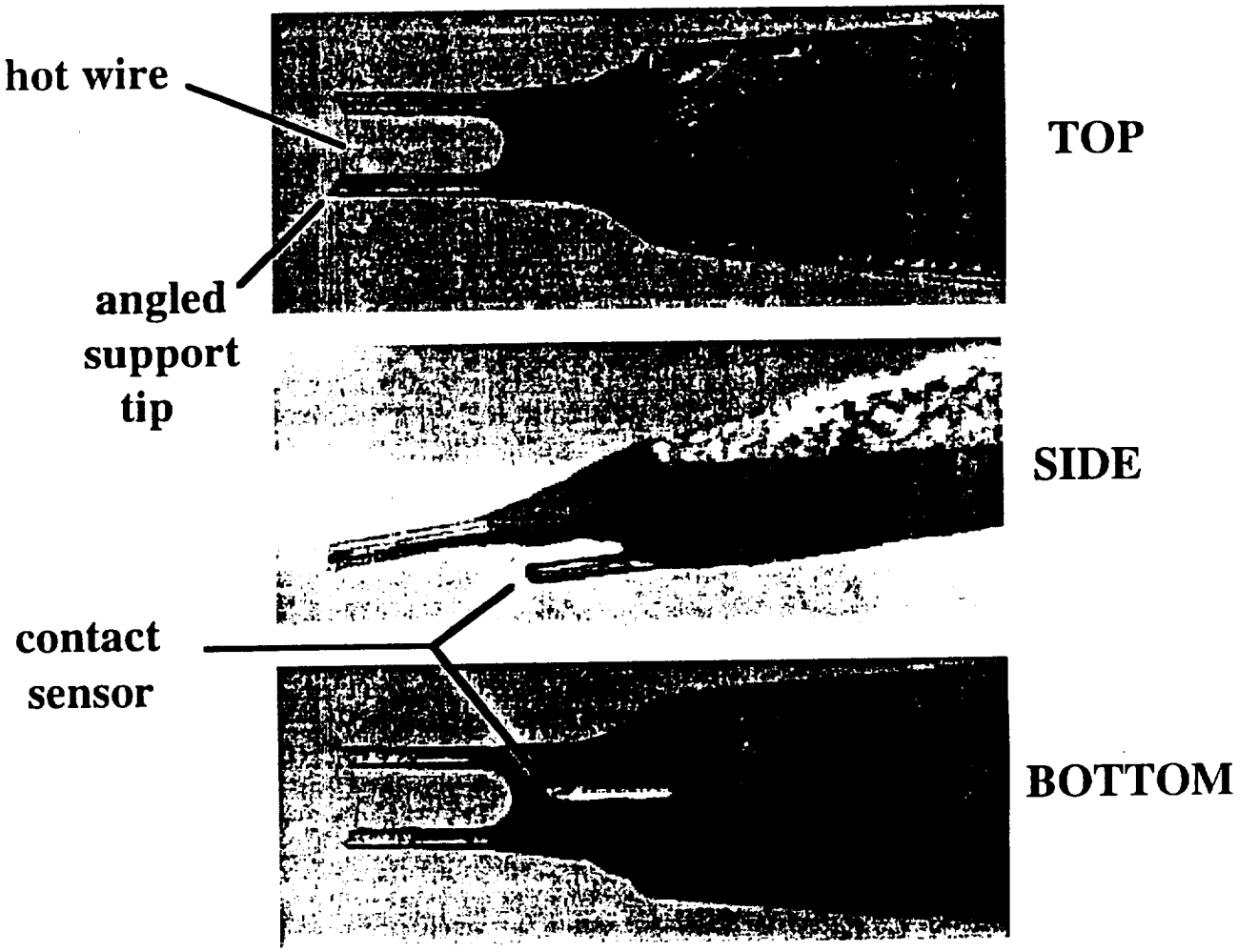

Alan E. Blanchard, Figure 3

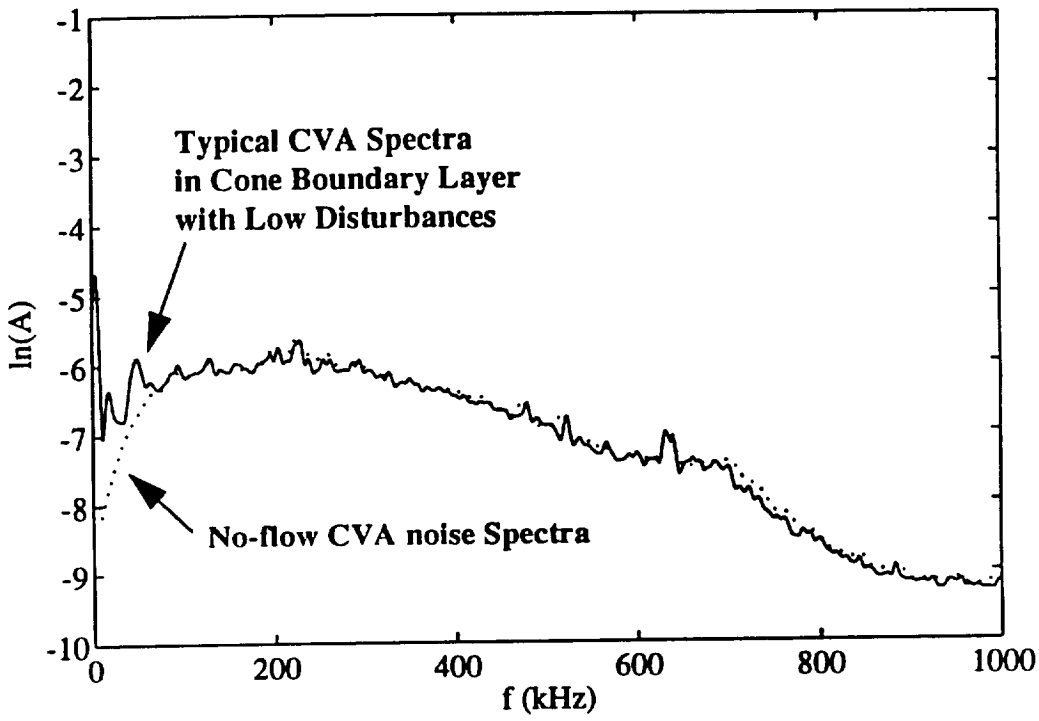

Alan E. Blanchard, Figure 4

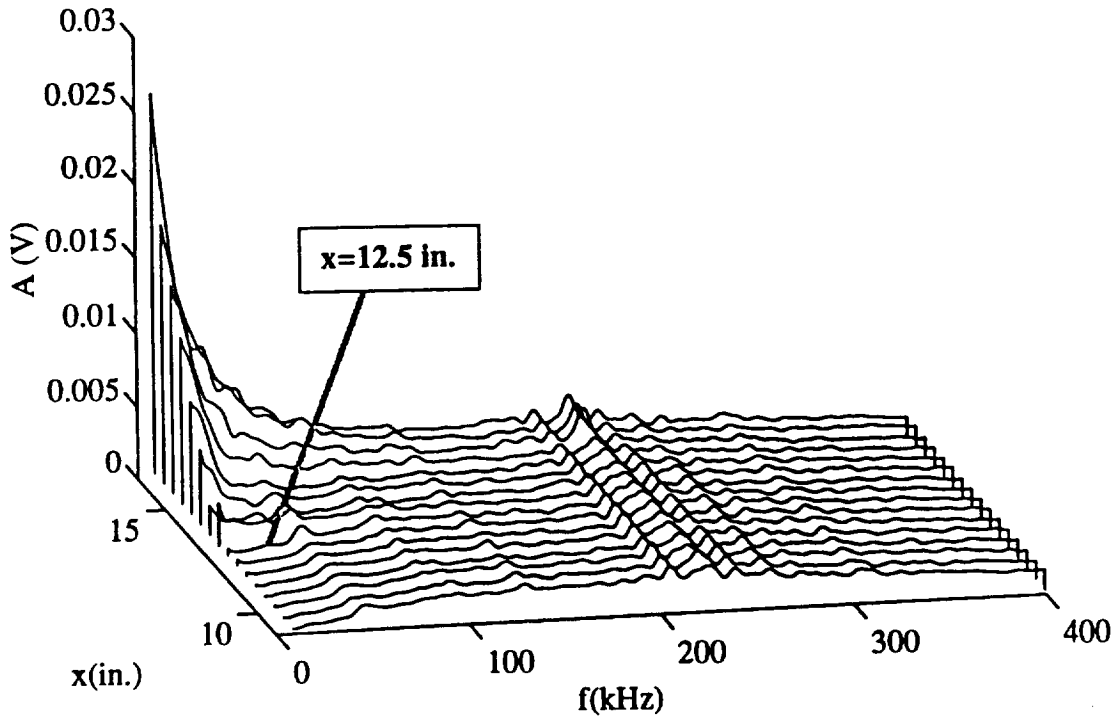

Alan E. Blanchard, Figure 5

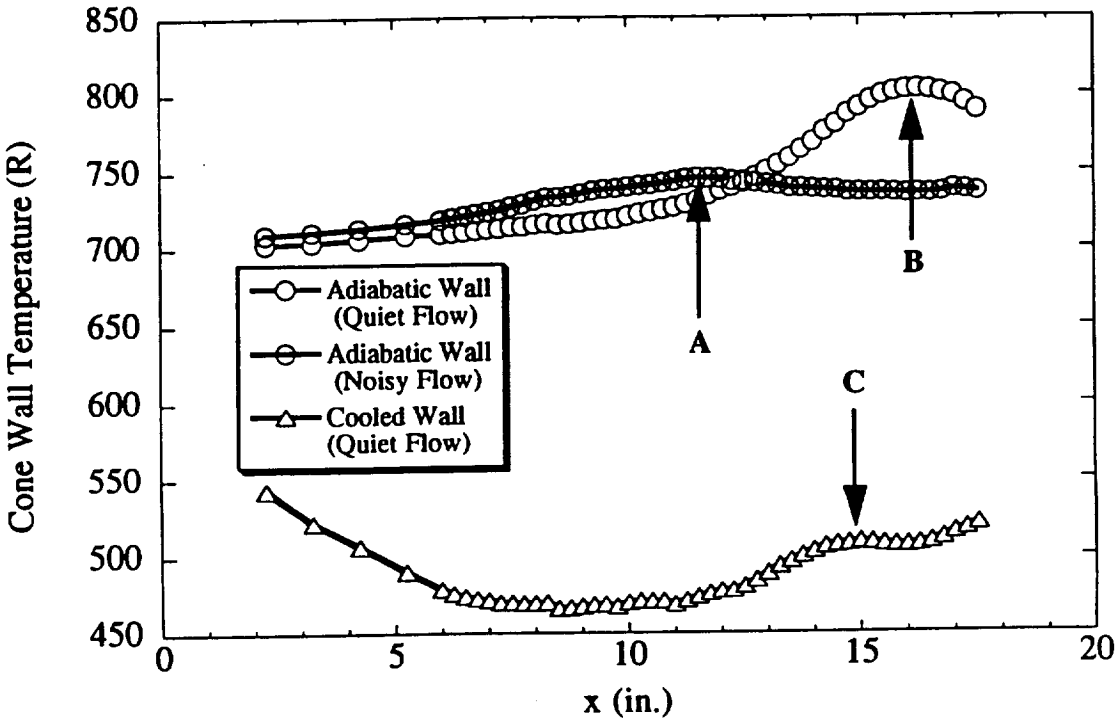

Alan E. Blanchard, Figure 6

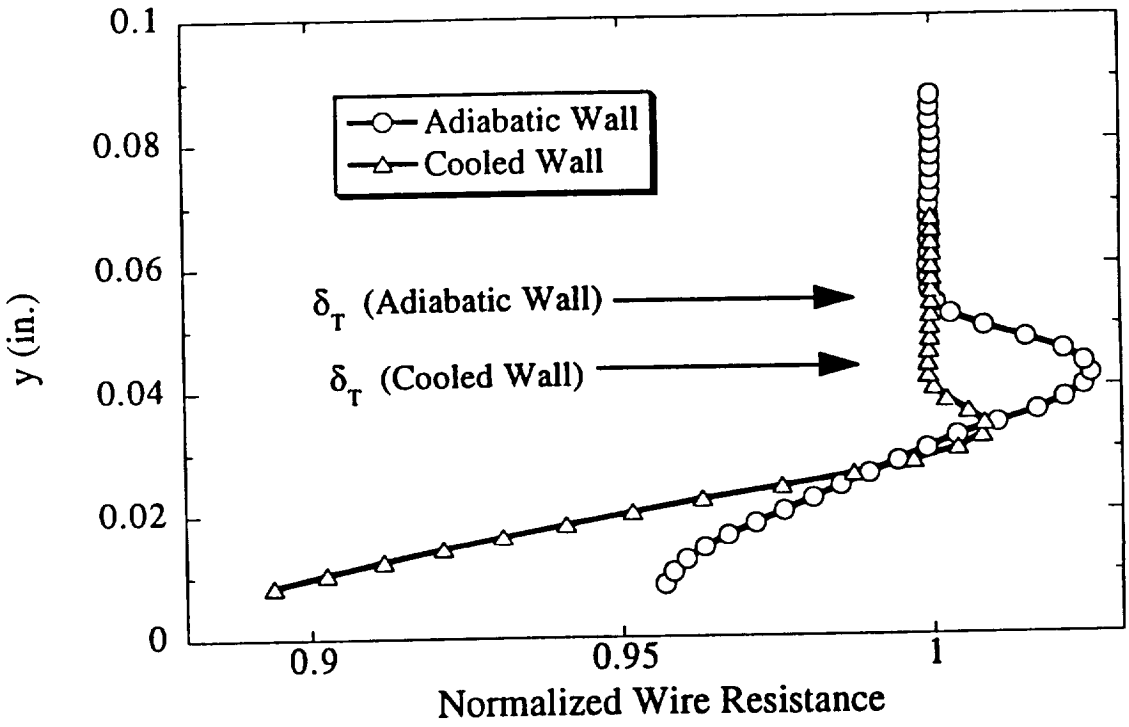

Alan E. Blanchard, Figure 7

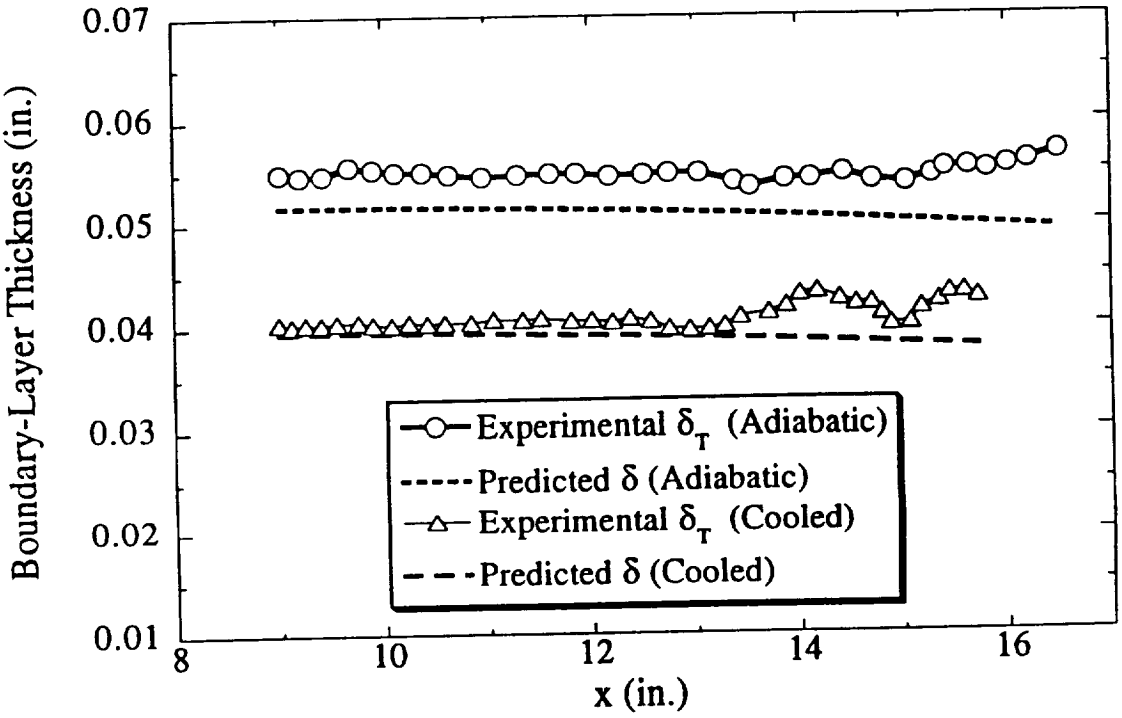

Alan E. Blanchard, Figure 8

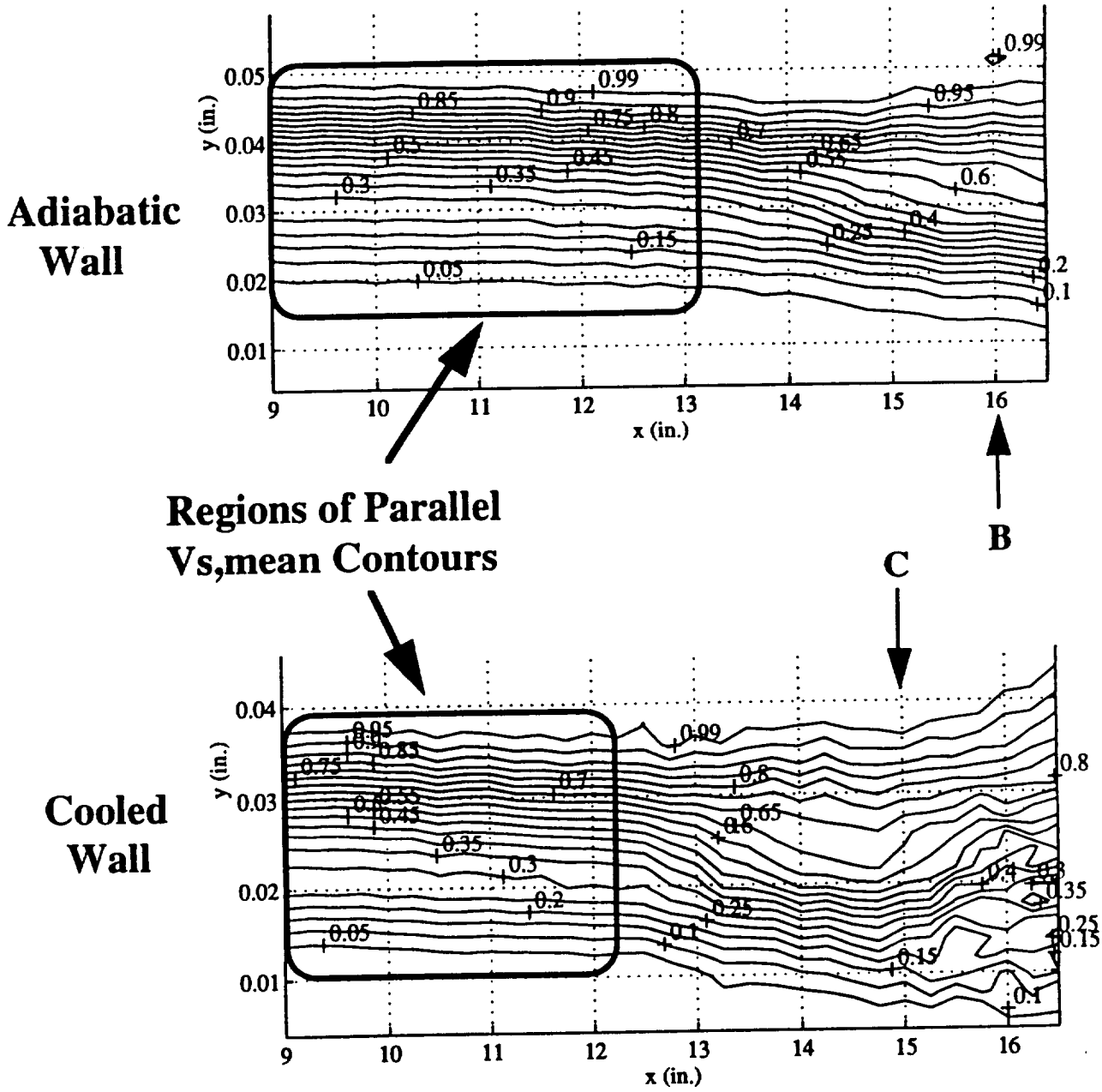

Alan E. Blanchard, Figure 9

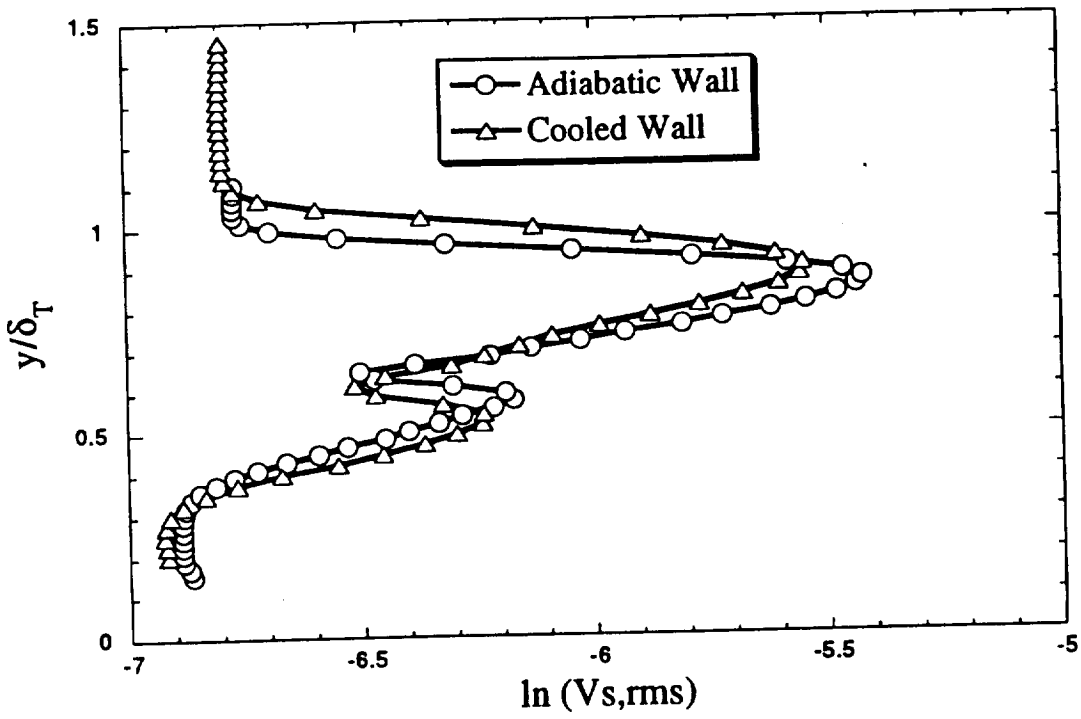

Alan E. Blanchard, Figure 10

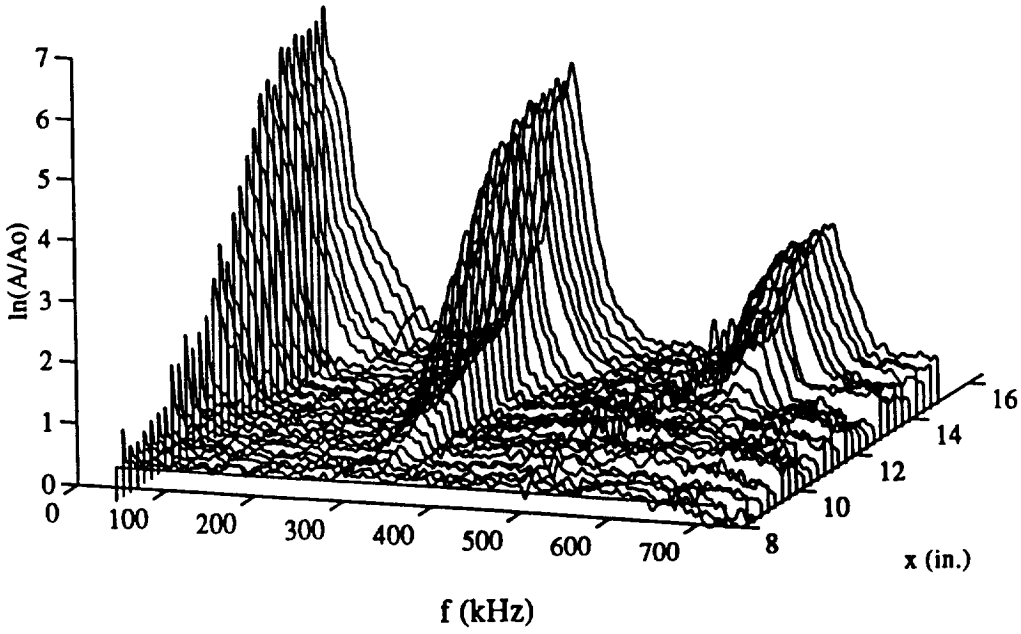

Alan E. Blanchard, Figure 11

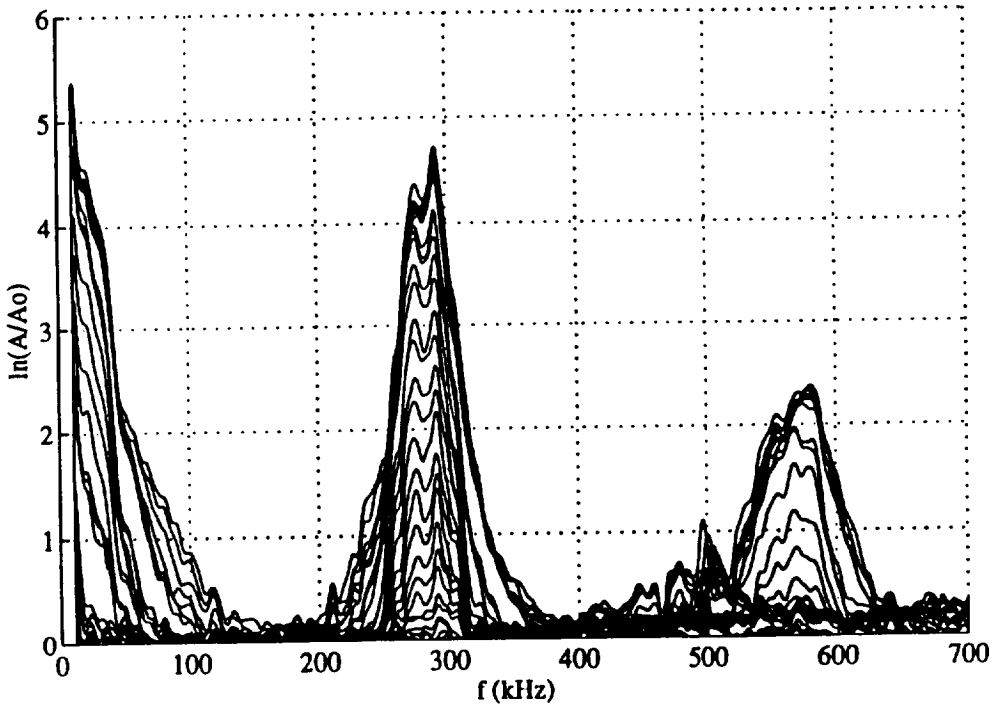

Alan E. Blanchard, Figure 12

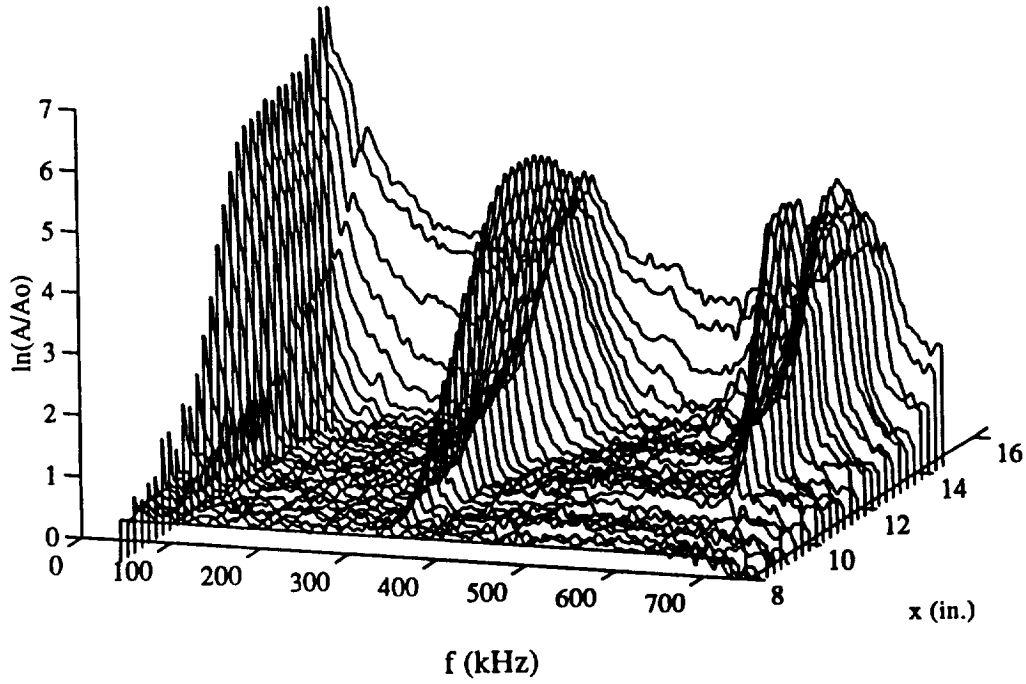

Alan E. Blanchard, Figure 13

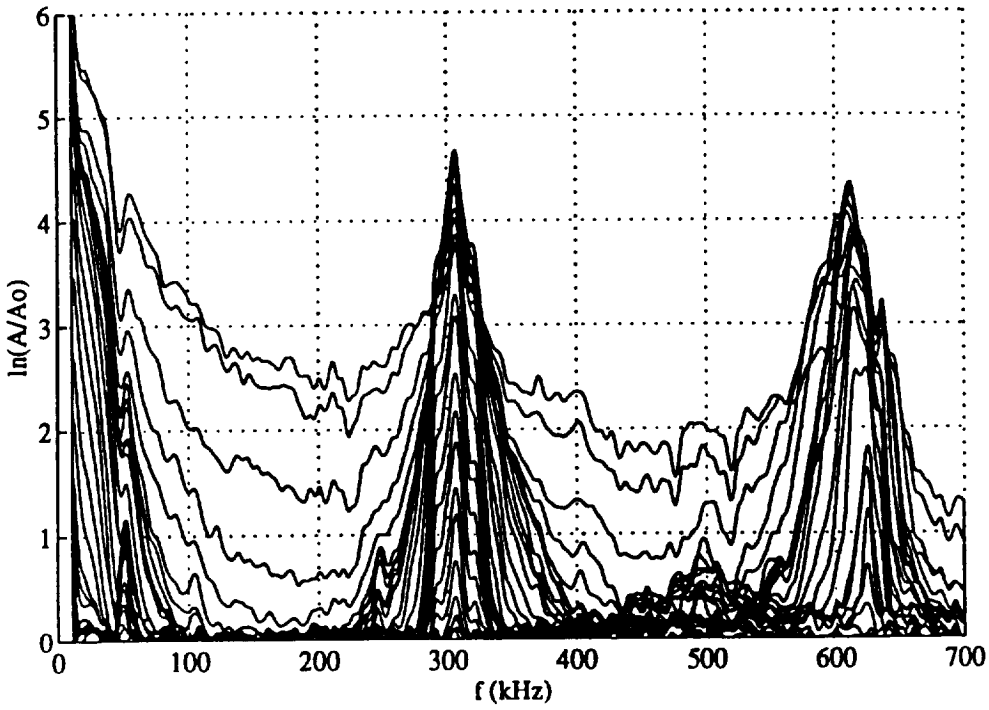

Alan E. Blanchard, Figure 14

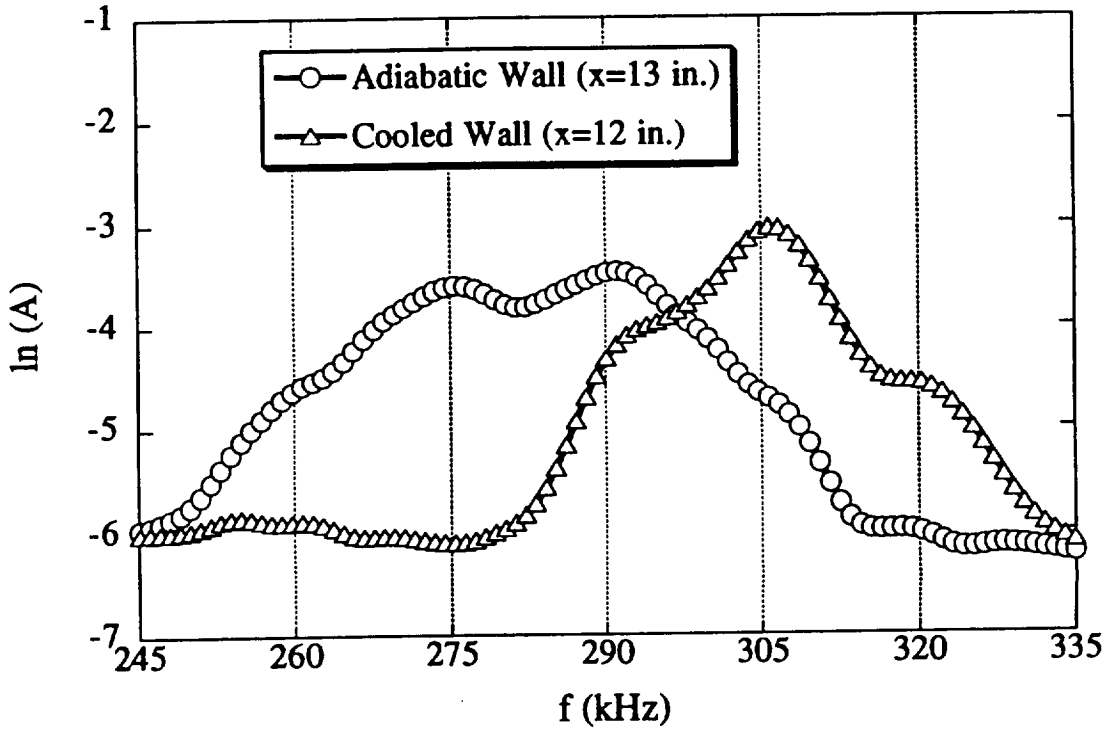

Alan E. Blanchard, Figure 15

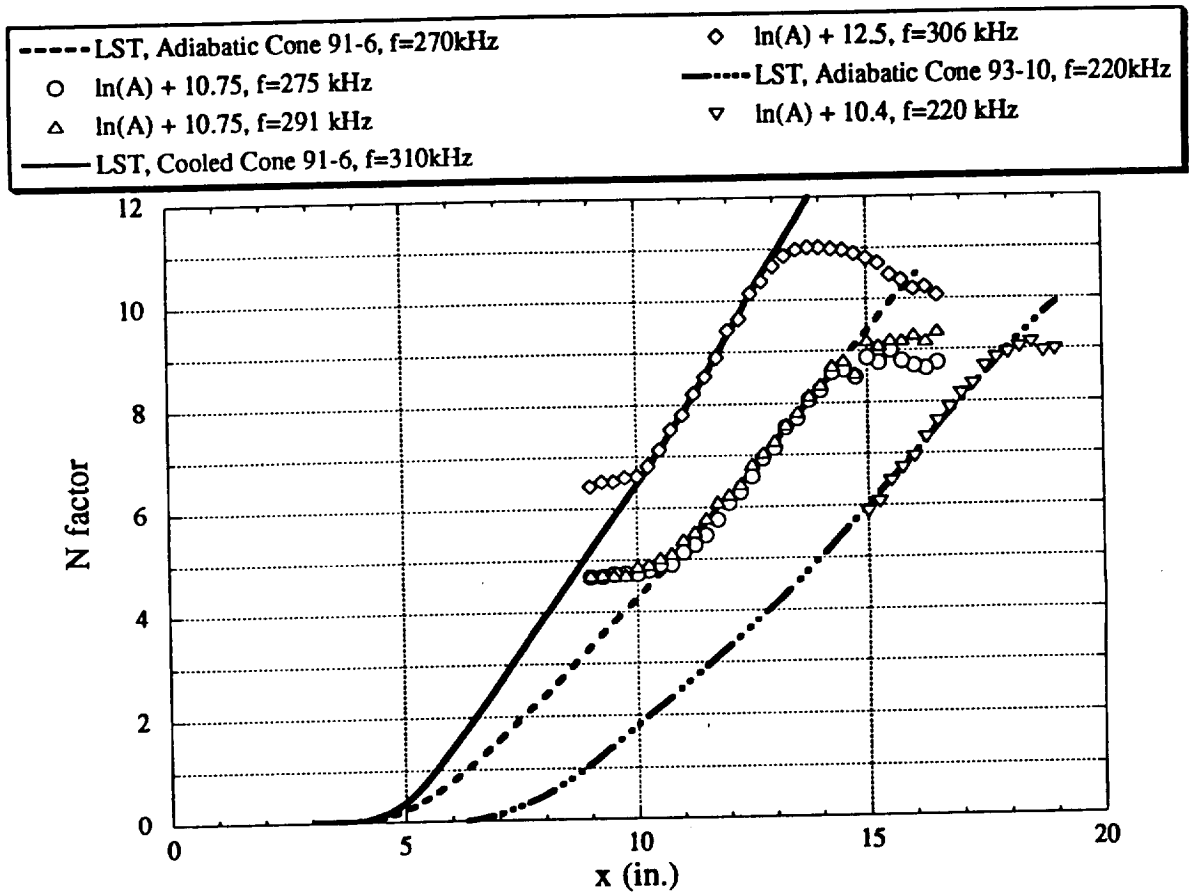

Alan E. Blanchard, Figure 16

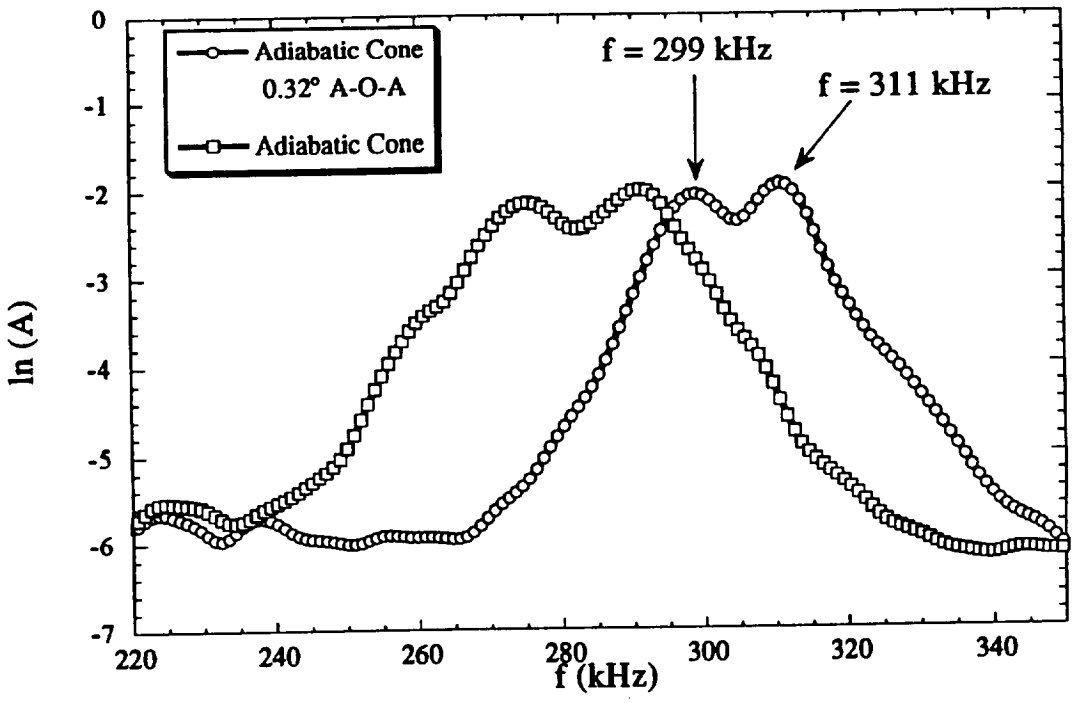

Alan E. Blanchard, Figure 17

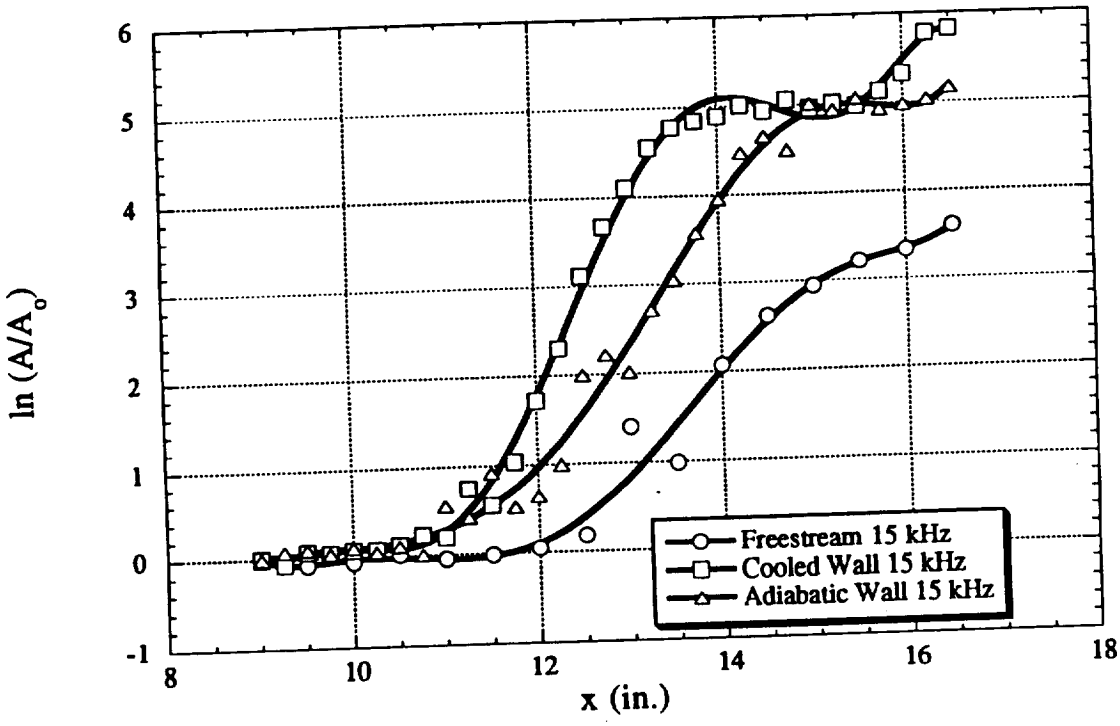

Alan E. Blanchard, Figure 18